J Nanostruct 15(3): 1121-1129, Summer 2025

RESEARCH PAPER

Fabrication and Photocatalytic Evaluation of Ag/SnO_2 Composites in the Treatment of Polluted Water

Adnan M. Mahdi

Ministry of Education, Open Educational College Wasit Study Centre Alsuwairah Branch, Iraq

ARTICLE INFO

Article History:
Received 10 April 2025
Accepted 19 June 2025
Published 01 July 2025

Keywords:
Ag/SnO_2 films
MB dye
Photocatalysis
Sol-gel technique
UV irradiation

ABSTRACT

Ag/SnO_2 films were fabricated over silicon (Si) (111) substrates by sol gel technique, and dipping method and evaluated for photocatalytic application to decompose methylene blue (MB). Structural, morphological, and optical measurements were investigated using XRD, AFM, SEM, and UV-Vis DRS spectroscopy. SEM images showed that the Ag/SnO_2 thin films were homogeneous and the particle size increased with increasing Ag doping content. The optical properties illustrated as Ag doping content increased, energy gap values of Ag/SnO_2 films reduced. Results showed the best Ag doping was 6wt%, with 82% degradation efficiency and obvious constant (k_{app}) of 9.68×10^{-3} min^{-1} after 3 h under UV irradiation.

How to cite this article
Mahdi A. Fabrication and Photocatalytic Evaluation of Ag/SnO_2 Composites in the Treatment of Polluted Water. J Nanostruct, 2025; 15(3):1121-1129. DOI: 10.22052/JNS.2025.03.030

INTRODUCTION

Many industrials release various organic and inorganic pollutants into the environment. These liquid or solid wastes contain oils, dyes, and various other chemicals that are harmful for the environment and threaten human life. Consequently, there is a need to develop advanced, environmentally friendly wastewater purification technologies before releasing pollutants into the environment. One of the most promising and advanced methods is the decomposition of organic pollutants such as dyes and other harmless substances using photocatalytic technology [1]. SnO_2 is one of the important semiconductor materials, attracting the interest of researchers as a photocatalytic material [2]. SnO_2 is a semiconductor with a direct bandgap of 3.6 to 4.0 eV, which depend on the preparation method and related conditions. This compound is used in a variety of fields, including electronics, sensors, detectors, cosmetics, and photocatalysts [2]. However, since visible light accounts for about 45% of radiation of solar energy, while ultraviolet light less than 10%, tin oxide is an excellent absorber of both ultraviolet and visible light in photocatalytic applications. To increase the photocatalytic activity, cations (transition metals) have been added to semiconductors in a number of studies to improve their properties and make them more suitable for photocatalytic applications [3, 4]. The performance and efficiency of photocatalyst can be improved by adding a metal to SnO_2 using a suitable doping material and preparation technique. For example, SnO_2 doped with Ag can be used in photocatalytic applications to improve the efficiency. In Ag/SnO_2, Ag ions have the ability to act as acceptors. The addition of Ag ions can enhance the absorption

* *Corresponding Author Email: dnanmshb7@gmail.com*

of wide window of light by reducing the bandgap of the semiconductor [5-7]. SnO_2 thin films can be produced using several preparation techniques, including metal oxide chemical vapor deposition (MOCVD) [8], sol-gel [9], spray pyrolysis [10], and pulsed laser deposition (PLD) methods [11]. Sol-gel is one of the most popular techniques due to its simplicity, lack of sophisticated equipment, controllability of film thickness, and high quality. In this work, we used sol-gel technique and dip-coating method to prepare Ag-doped SnO_2 thin films for photocatalytic purposes. We used MB dye as a water contaminant for the study. This research aimed to evaluate the high concentration of Ag substitution in SnO_2 and the degradation potential of MB.

MATERIALS AND METHODS

Sol-gel dip coating is used to deposit Ag/SnO_2 thin films on silicon (Si) (111) substrates. To get 0.1 M sol in absolute ethanol (99.9%), tin (II) acetate ($Sn(C_2H_3O_2)_2$, Merck, purity 99%) and silver nitrate ($AgNO_3$, Merck, purity > 97.0%) were utilized. Tin (II) sol was initially prepared by dissolving an appropriate amount of $Sn(C_2H_3O_2)_2$ in ethanol using a magnetic stirrer for three h at 80 °C. A appropriate amount of $AgNO_3$ was dissolved in ethanol and agitated for 2 h at room temperature to create [Ag]⁄([Sn] + [Ag]) =4 mol% Ag-doped solution. Then, two solutions were mixed for 1 h at room temperature. The thin films were obtained using dip coating with a withdrawal speed of 15 cm/min. The coating films were dried for 15 min at 100 °C. Ten iterations of the thin film deposition and drying procedures were carried out. The as-deposited samples were then annealed in atmosphere for 2 h at 550 °C. The photocatalytic test was accomplished by an aqueous MB solution (λ = 664 nm) under UV (15 W UV tube, Aquake). The solution of MB dye was 40 mL and specimens were irradiated with UV source. The degradation of the MB dye was measured using the absorption spectra at orderly period (each 30 min) by a UV-Vis spectroscopy (Shimadzu 1245 SAB). The MB degradation efficiency (η) was evaluated using equation [4]:

$$\eta = \frac{(C_o - C_t)}{C_o} \times 100 \quad (1)$$

where the starting concentration is denoted by C_o and the concentration following t min of photocatalysis is introduced by C_t.

The thickness of obtained films was measured by an optical interferometer method; the thickness was 260, 265, 256, and 264 nm for Ag/SnO_2 thin films at 0, 2, 4, and 6 wt% Ag, respectively. To display the attributes of the structure, PW1841 Philips was used for the X-ray diffraction (XRD, Cu−Kα, λ=0.154 nm). A Shimadzu 1245 SA UV/Vis spectroscopy was used to record the optical characteristics. The MIRA3 TESCAN-XMU FESEM device was used to identify the surface morphology.

RESULTS AND DISCUSSION

Fig. 1 showed the XRD patterns of the SnO_2 thin films doped with Ag at 0, 2, 4, and 6 wt%. The peaks recorded for the diffraction patterns were appeared at angles of 31.16°, 36.34°, 51.01°, and 66.43°, which are related to the (111), (200), (220), and (222) phase, respectively. These results indicate that prepared films consist of nanoparticles with a tetrahedral network, which is consistent with JCPDS cards 43-1038 and 33-1374. It can be observed that with increasing silver concentration, the dominant reflection peak of (111) decreases, indicating that the SnO_2 particles have been deposited in non-substituted interfacial sites [12]. Also, it can be observed that the Ag diffraction peaks gradually appear with increasing Ag concentrations from 2 to 6 wt% (JCPDS card No. 04-0783), indicating the entry of Ag particles into the SnO_2 crystalline structure, where new peaks appeared at 40.64° and 51.01° corresponds to the (201) and (302) phase of AgO, respectively. The emergence of AgO phase led to a reduction in the crystal size and thus will increase the photocatalytic efficiency of the Ag/ SnO_2 particles [13]. To calculate the crystallite size, the Debye-Scherrer formula [14] was used at the (111) plane (Table 1), as follows:

$$D = \frac{K\lambda}{\beta \cos\theta} \quad (2)$$

where θ represent diffraction angle, K represent constant value (0.9), β represent full width at half maximum (FWHM) of the peak in radians, and λ (1.54 Å) represent the wavelength of the X-ray beam. We observe that the crystallite size decreases when the silver concentration increases to 6 wt%, which can be attributed to the stress resulting from the difference in ion size between silver and tin [15].

Fig. 2 provides a good illustration of the SnO_2 film structure, showing prepared films with good surface homogeneity. We observe that the doping with particles creates a more uniform particle distribution in the prepared film, altering the particle size, changing the atomic positions, and causing recrystallization. The smoothness of the films can be attributed to the arrangement of surface atoms to produce a secondary energy state. The small spherical grains cluster to express the Ag doping, resulting in an extremely smooth surface with little roughness. Results in terms of grain distribution and roughness are summarized in Table 2, which shows that the film grain size, roughness, and root mean square (RMS) ratios decrease with increasing silver doping ratios. Consequently, as the grain size decreases, the film roughness increases [16].

FESEM analysis was employed to examine the surface morphology of the Ag/SnO_2 thin films. FESEM images of samples on Si substrates were displayed in Figs. 3(a-d). The surface of the films varies with concentration of Ag. We discovered that the surface of SnO_2 has a shape resembling strings. The surface of the SnO_2:2wt%Ag film is not uniform, but the SnO_2:4wt%Ag film exhibits a large number of uniformly sized particles. The nonuniform surface of the SnO_2:6wt%Ag film

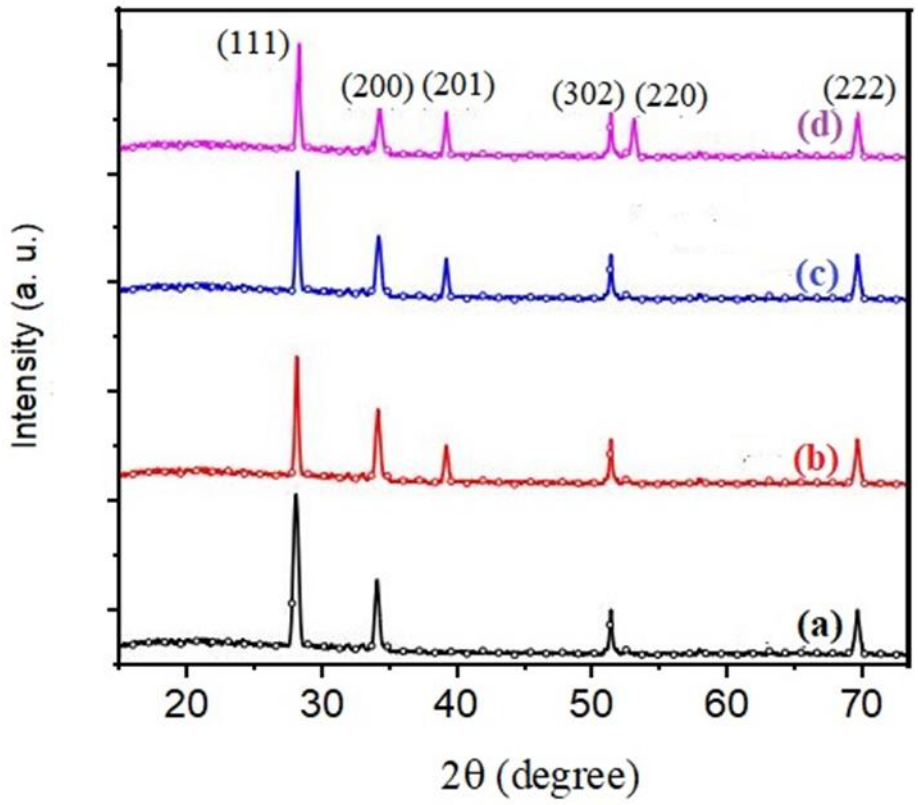

Fig. 1. XRD patterns of (a) pure SnO_2, (b-d) SnO_2 thin films doped with Ag at 2, 4, and 6 wt%.

Table 1. XRD data of resulting SnO_2 and Ag/SnO_2 thin films.

Samples	2θ	FWHM (θ)	Crystallite Size (nm)
SnO_2	31.164	0.3304	24.746
SnO_2:2wt%Ag	31.162	0.3721	23.883
SnO_2:4wt%Ag	31.159	0.3578	22.855
SnO_2:6wt%Ag	31.158	0.3643	22.446

was also demonstrated. Result of photocatalytic activity can be affected by surface morphology.

The absorbance spectra of SnO_2 and Ag/SnO_2 thin films coated on Si (111) substrates were displayed in Fig. 4. It is evident that when Ag concentrations rise, the absorption edge shifts to higher wavelengths, ranging from 300 to 400 nm.

The transmittance spectra of SnO_2 and Ag/SnO_2 thin films are displayed in Fig. 5. As the Ag concentration rises, transmittance intensity of Ag/SnO_2 thin films drop from around 90% to 30% in the visible area. Grain boundary scattering can reduce the transmittance value. Fig. 6 displays the associated curves for as-obtained samples. For SnO_2, the optical band gap energy is 4.07 eV. The ranges of 3.95 to 4.04 eV were recorded for Ag/SnO_2 thin films. As the amount of Ag in composite sample increased, the band gap value reduced [17].

When Ag/SnO_2 thin films are irradiated with light energy greater than the bandgap energy of films, photocatalytic activity begins. The valence band forms holes (h^+) and the conduction band forms electrons (e^-). Electrons are then produced as superoxide ($O_2\bullet^-$) and other reactive oxygen species (H_2O_2 and •OH), while the holes interact with water to form •OH. As a result, organic bonds and the oxidizing capacity of •OH radicals can break the C–C and C–H bonds of the MB on the surface of Ag/SnO_2 films, producing CO_2 and H_2O [18]. After being submerged in 40 mL of MB (10 ppm), thin films were exposed to UV (A) light for 3 h. UV/Visible spectroscopy was used to measure the absorption spectra of MB dye after each irradiation cycle to calculate the photodegradation of MB dye during UV exposure. Fig. 7 shows

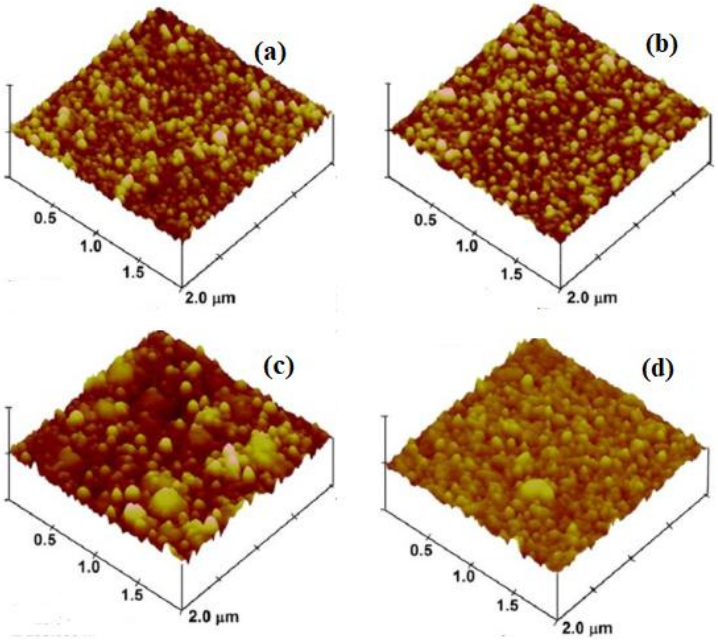

Fig. 2. AFM graphs of (a) pure SnO_2, (b-d) SnO_2 thin films doped with Ag at 2, 4, and 6 wt%.

Table 2. AFM data of resulting SnO_2 and Ag/SnO_2 thin films.

Samples	Grain size (nm)	Roughness (nm)	RMS (nm)
SnO_2	98.77	0.764	0.638
SnO_2: 2wt%Ag	93.97	0.413	0.412
SnO_2: 4wt%Ag	80.51	0.396	0.327
SnO_2: 6wt%Ag	78.95	0.379	0.316

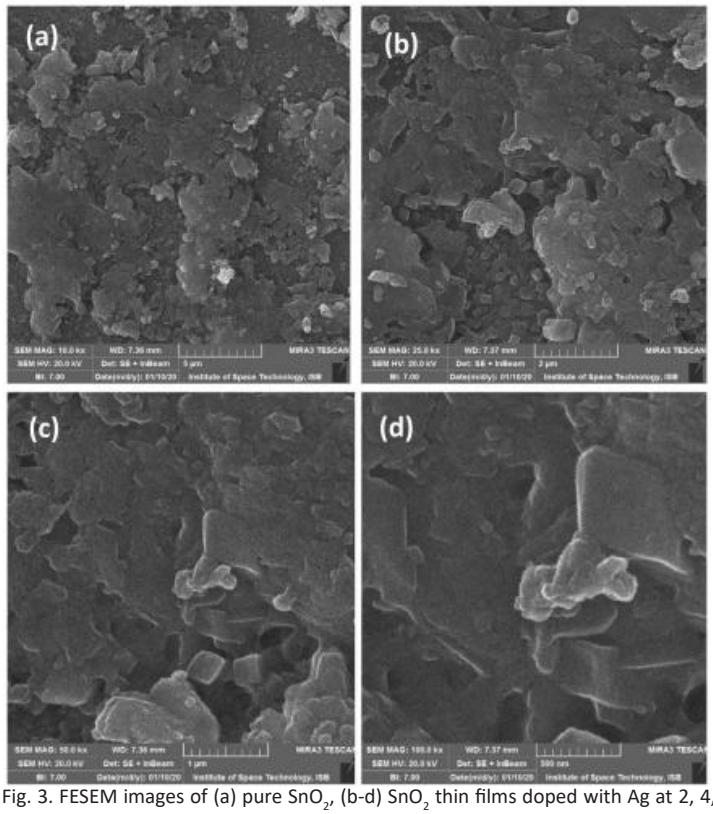

Fig. 3. FESEM images of (a) pure SnO_2, (b-d) SnO_2 thin films doped with Ag at 2, 4, and 6 wt%.

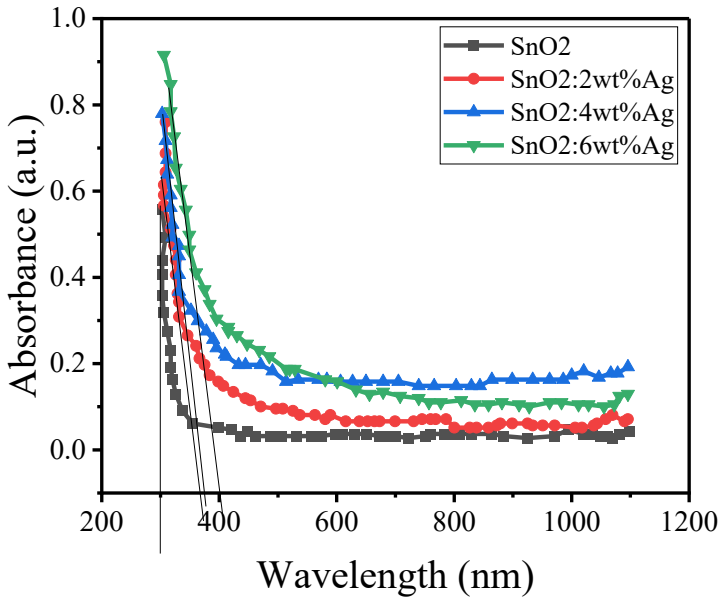

Fig. 4. Absorbance spectra of SnO_2 and Ag/SnO_2 thin films.

the relationship between irradiation time and concentration difference (Ci/Co). It is evident that after 3 h, the photodegradation of MB by Ag/SnO_2 thin films can reach 82%, while MB dye in water without photocatalyst yield about 17%. These results indicates that MB does not change significantly in the absence of photocatalysts. Ag actively forms hydroxyl radicals on the surface

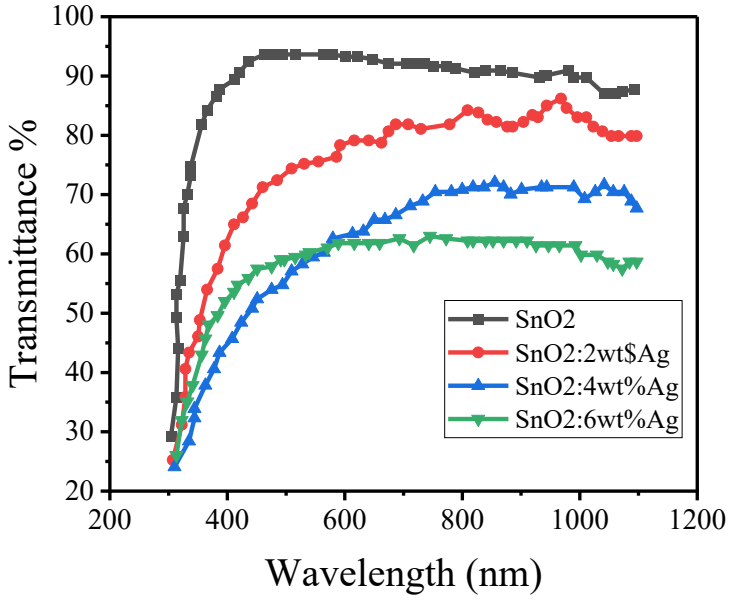

Fig. 5. Transmittance spectra of SnO_2 and Ag/SnO_2 thin films

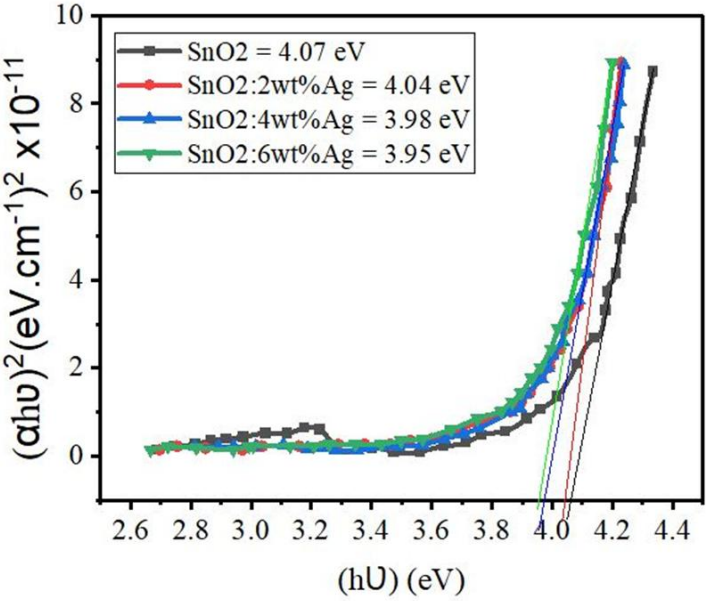

Fig. 6. The plots of $(ahv)^2$ as a function of (hv) for SnO_2 and Ag/SnO_2 thin films.

of SnO_2 thin films, describing high photoactivity [19]. In addition, the surface plasmon resonance (SPR) effect also had an effect. SPR can enhance photoactivity by increasing light absorption and charge carrier separation upon exposure to UV light [20, 21].

The kinetics of MB is described by the Langmuir-Hinshelwood model, and related rate (r) calculated as below [22]:

$$r = -\frac{dC}{dt} = \frac{k_r K_{day} C}{1 + K_{day} C} \quad (3)$$

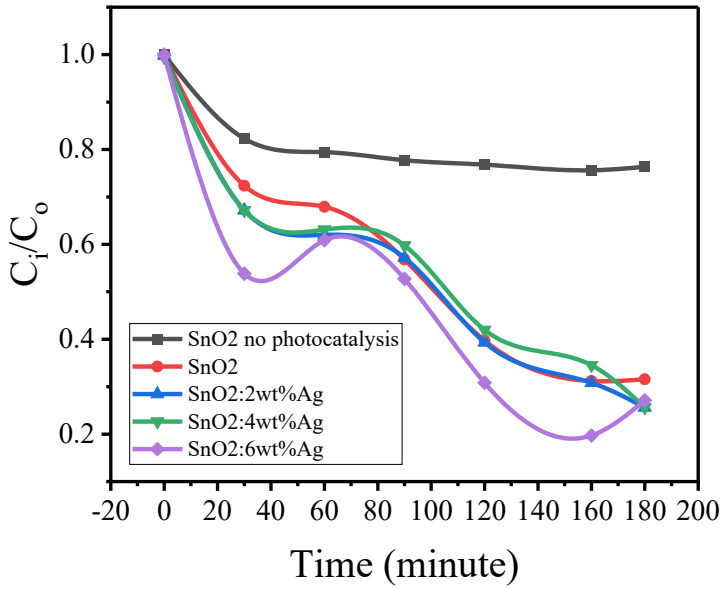

Fig. 7. The MB dye degradation under UV irradiation for SnO_2 and Ag/SnO_2 thin films.

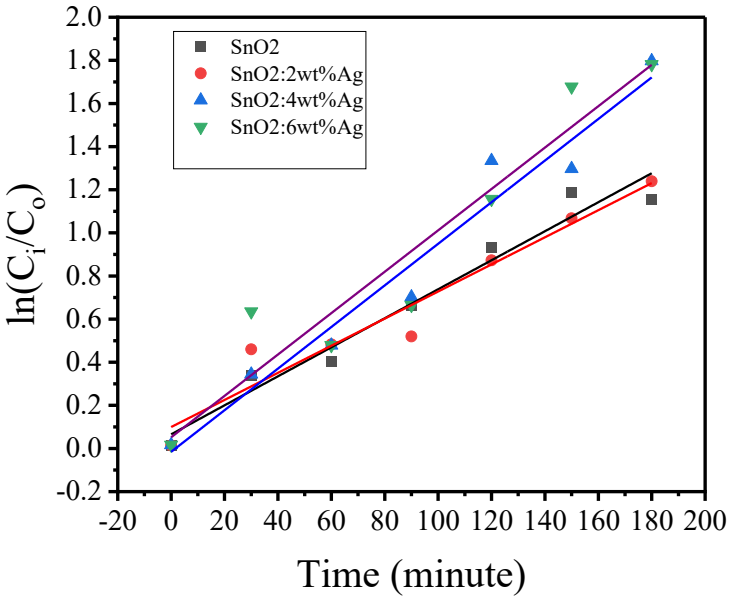

Fig. 8. The kinetic of MB dye degradation under UV irradiation for SnO_2 and Ag/SnO_2 thin films.

Table 3. The rate constants (*K*) of MB dye degradations.

Samples	$K_{app} \times 10^{-3}(min)^{-1}$	R^2
SnO_2	6.73	0.94
SnO_2:2wt%Ag	6.29	0.94
SnO_2:4wt%Ag	9.65	0.95
SnO_2:6wt%Ag	1.29	0.80

where the dye concentration (mg/L^{-1}) at irradiation time (t) is represented by C, the degradation rate (mg/L^{-1} min^{-1}) is represented by *dC/dT*, the rate constant (min^{-1} g/L^{-1}) is k_r, and the dye adsorption coefficient (mg^{-1}) is K_{dye}. At a first-order apparent rate constant k_{app} (min^{-1}) and low concentrations ($K_{dye}C \ll 1$), equation (4) reduces to a first-order kinetic model [23]:

$$\ln\left(\frac{C_i}{C_o}\right) = -k_r K_{dye} t = -k_{app} t \quad (4)$$

The slopes of the linear plots of ln(*C*i/*C*o) over time (t) yield the constants $k$app of MB (Table 3). The results showed that the maximum apparent first-order rate constant ($k$app) for Ag/SnO_2 thin films was about 9.68×10^{-3} min^{-1}, and the correlation coefficient was about 0.94, as shown in Fig. 8. These results are consistent with those of Babu et al. [24].

CONCLUSION

Sol gel and dipping techniques have been used to create Ag/SnO_2 thin films onto Si (111) substrates for photocatalysis applications. The films feature a polycrystalline phase, according to XRD examination. Each Ag doping concentration displayed a distinct shape in the SEM images. The optical characteristics of Ag/SnO_2 thin films were investigated by increasing Ag concentrations. About 3.95 eV was the lowest energy gap found in SnO_2:6wt%Ag film. Under UV light irradiation, the degradation of MB solution was examined in the presence of Ag/SnO_2 thin films. The most effective sample for MB photodegradation was SnO_2: 6wt%Ag thin film.

ACKNOWLEDGMENT

The authors would like to thank the Scientific Research commission Ministry of Higher Education Baghdad-Iraq for facilitate work to complete this research.

CONFLICT OF INTEREST

The authors declare that there is no conflict of interests regarding the publication of this manuscript.

REFERENCES

1. Shuvo MSH, Putul RA, Hossain KS, Masum SM, Molla MAI. Photocatalytic Removal of Metronidazole Antibiotics from Water Using Novel Ag-N-SnO_2 Nanohybrid Material. Toxics. 2024;12(1):36.
2. Ag/Ag_2S Nanoparticle-Induced Sensitization of Recovered Sulfur-Doped SnO2 Nanoparticles for SO_2 Detection. American Chemical Society (ACS).
3. Roy H, Rahman TU, Khan MAJR, Al-Mamun MR, Islam SZ, Khaleque MA, et al. Toxic dye removal, remediation, and mechanism with doped SnO2-based nanocomposite photocatalysts: A critical review. Journal of Water Process Engineering. 2023;54:104069.
4. Chawla A, Sudhaik A, Raizada P, Khan AAP, Singh A, Van Le Q, et al. An overview of SnO_2 based Z scheme heterojuctions: Fabrication, mechanism and advanced photocatalytic applications. Journal of Industrial and Engineering Chemistry. 2022;116:515-542.
5. Jain SK, Fazil M, Naaz F, Pandit NA, Ahmed J, Alshehri SM, et al. Silver-doped SnO_2 nanostructures for photocatalytic water splitting and catalytic nitrophenol reduction. New J Chem. 2022;46(6):2846-2857.
6. Zhang Q, Zou X, Wang Y, Habibi M. Study on photocatalytic, electric, and sensing behavior of Co- and Ag-codoped tin dioxide (SnO_2) nano particles. Materials Science and Engineering: B. 2023;296:116687.
7. Gangwar K, Jeevanandam P. Synthesis of SnO_2-Ag nanocomposites via thermal decomposition method and their application for catalytic reduction of 4-nitrophenol and photocatalytic degradation of congo red. J Mol Struct. 2023;1285:135423.
8. Rodríguez-López J, Rangel R, Lara-Romero J, Quintana-Owen P, Bartolo-Pérez P, Ramos-Carrazco A. Structural parameters determination of ALD-SnO2 thin films grown on silicon (100) and boron-doped silicon (100) substrates. Journal of Ovonic Research. 2024;20(5):627-632.
9. Aydın Ünal F. Synthesis and characterization of the doped/co-doped SnO_2 nanoparticles by the sol–gel method. International Journal of Applied Ceramic Technology. 2024;22(1).
10. Ismael MI, Ali GG, Zakar AT. Synthesis and characterization of SnO_2/porous silicon hybrid nanostructures for gas sensing. Journal of Ovonic Research. 2024;20(6):851-865.
11. Aldaghri O. Enhancing UV photodetection sensitivity via pulsed laser optimization in SnO_2:WO_3/Si nanostructures. Journal of Optics. 2024;26(12):125002.

12. Rzaij JM, Abbas QA, Khalaf AM. Investigating the structural, topographical, morphological and optical effects of AgO on sprayed SnO2 thin films. Bull Mater Sci. 2023;46(4).
13. Liang Y-C, Hsu Y-W. Design of thin-film configuration of SnO_2–Ag_2O composites for NO_2 gas-sensing applications. Nanotechnology Reviews. 2022;11(1):1842-1853.
14. Kajal R, Kandasami A, Kataria B, Solanki P, Mohan D. Structural, optical, and dielectric characteristics of pulsed laser deposited SnO_2-TiO_2 composite thin films. Phys Scr. 2023;98(8):085935.
15. Chouhan L, Panda SK, Bhattacharjee S, Das B, Mondal A, Parida BN, et al. Room temperature d0 ferromagnetism, zero dielectric loss and ac-conductivity enhancement in p-type Ag-doped SnO_2 compounds. J Alloys Compd. 2021;870:159515.
16. Hassun HK, Hussein BH, Salman EMT, Shaban AH. Photoelectric properties of SnO_2: Ag/P–Si heterojunction photodetector. Energy Reports. 2020;6:46-54.
17. Xu S, Li D, Guo J, Hu Y, Yang P. Aluminum and silver doped effects on the electrical structure and optical properties of SnO_2. Journal of Physics and Chemistry of Solids. 2021;148:109763.
18. Boudechiche N, Sadaoui Z, Trari M, Canle M. The photosensitization and photocatalytic activity of the n-ZnO/p-$CuAl_2O_4$ hetero-system for degradation of two dyes under visible light. Chem Eng Commun. 2025;212(7):1048-1066.
19. Liu J, Yao H, Zhang K, Xue S, Fang D, Zhang H, et al. In-situ immobilization of a novel fixed Z-scheme Ag|Ag_2S/Ag/SnO_2 photocatalytic system for pure hydrogen production and synchronous tartrazine degradation: Efficiency and mechanism insight. Journal of Environmental Chemical Engineering. 2025;13(2):115445.
20. Sun X, Liu J, Yang R, Gu H, Chen B, Wang C, et al. Surface plasmon resonance effect cooperated with Z-scheme heterostructure for enhancing photocatalytic nitrogen reduction to ammonia. Journal of Colloid and Interface Science. 2025;678:67-75.
21. Xu Q, Sun F, Liu X, Hu Y, Luo C, Wang X, et al. Upconverting luminescence and surface plasmon resonance synergistically boost photocatalytic activity of LaOCl:Yb^{3+},Er^{3+}/Bi_2MoO_6/Ag nanofiber S-scheme heterojunction photocatalyst for degradation of organic contaminants. J Alloys Compd. 2025;1020:179363.
22. Li X, Liu Y, Yao M, Liu F. N-doped sites modulate Ag/TiO_2 interaction for improved photocatalytic degradation of tetracycline. Molecular Catalysis. 2025;573:114815.
23. Huo Z, Xie X, Liu J, Chen F, Cao J, Sun W, et al. Engineering a Ru(ii) Nanostructure for Oxygen-Free Photocatalytic Degradation of Environmental Pollutants. ACS Applied Materials and Interfaces. 2025;17(12):18493-18501.
24. Babu B, Cho M, Byon C, Shim J. One pot synthesis of Ag-SnO_2 quantum dots for highly enhanced sunlight-driven photocatalytic activity. J Alloys Compd. 2018;731:162-171.